Cell Calcium 83 (2019) 102060

Contents lists available at ScienceDirect

Cell Calcium

journal homepage: www.elsevier.com/locate/ceca

The synthesis and characterization of a clickable-photoactive NAADP analog active in human cells

Timnit Yosef Asfaha[a], Gihan S. Gunaratne[b], Malcolm E. Johns[b], Jonathan S. Marchant[c], Timothy F. Walseth[b,**], James T. Slama[a,*]

[a] Department of Medicinal and Biological Chemistry, University of Toledo College of Pharmacy and Pharmaceutical Sciences, 3000 Arlington Avenue, Toledo, OH, 43614, United States
[b] Department of Pharmacology, University of Minnesota Medical School, 312 Church St., Minneapolis, MN, 55455-0217, United States
[c] Department of Cell Biology, Neurobiology & Anatomy, Medical College of Wisconsin, 8701 Watertown Plank Road, Milwaukee, WI, 53226-0509, United States

ARTICLE INFO

Keywords:
Calcium intracellular release
Chemical biology
Click chemistry
Nucleoside/nucleotide analogue
Photoaffinity labeling
Receptor
Sea urchin
Second messenger

ABSTRACT

Nicotinic acid adenine dinucleotide phosphate (NAADP) is a potent Ca^{2+} mobilizing second messenger which triggers Ca^{2+} release in both sea urchin egg homogenates and in mammalian cells. The NAADP binding protein has not been identified and the regulation of NAADP mediated Ca^{2+} release remains controversial. To address this issue, we have synthesized an NAADP analog in which 3-azido-5-azidomethylbenzoic acid is attached to the amino group of 5-(3-aminopropyl)-NAADP to produce an NAADP analog which is both a photoaffinity label and clickable. This 'all-in-one-clickable' NAADP (AIOC-NAADP) elicited Ca^{2+} release when microinjected into cultured human SKBR3 cells at low concentrations. In contrast, it displayed little activity in sea urchin egg homogenates where very high concentrations were required to elicit Ca^{2+} release. In mammalian cell homogenates, incubation with low concentrations of [^{32}P]AIOC-NAADP followed by irradiation with UV light resulted in labeling 23 kDa protein(s). Competition between [^{32}P]AIOC-NAADP and increasing concentrations of NAADP demonstrated that the labeling was selective. We show that this label recognizes and selectively photodervatizes the 23 kDa NAADP binding protein(s) in cultured human cells identified in previous studies using [^{32}P]5-N_3-NAADP.

1. Introduction

Changes in intracellular calcium regulate diverse processes such as metabolism, secretion, proliferation, muscle contraction, learning and memory and cell death [1–5]. Intracellular Ca^{2+} release can be triggered by diffusible second messengers, inositol-1,4,5-trisphosphate (IP3)[1], cyclic ADP-ribose (cADPR) and nicotinic acid adenine dinucleotide phosphate [6,7] (NAADP, structure **1** in Fig. 1), and these changes are amplified by Ca^{2+} itself through the process of calcium-induced calcium release. NAADP is a very close structural analogue of the more familiar pyridine dinucleotide $NADP^+$ in which the nicotinamide moiety is replaced by nicotinic acid. This modest change in structure results in profound changes in biological activity, changing the biological activity of NADP from a redox active co-substrate to the second messenger activity of NAADP [8–10].

The Ca^{2+} mobilizing activity of NAADP has been confirmed in many different cell types. NAADP effectively mobilizes Ca^{2+} at very low concentrations (an EC_{50} of approximately 10–50 nM when measured using sea urchin egg homogenates [7] and ascidian oocytes [11]). Although mammalian cell homogenates do not respond to NAADP, mammalian cells – for example, mouse pancreatic acinar cells – also release Ca^{2+} in response to low concentrations of microinjected NAADP [12]. NAADP has been shown to be involved in the fertilization process in sea urchin eggs [13,14], in smooth muscle contraction in several tissues [15], in mediating neuronal functions [16], and in regulating insulin secretion from pancreatic β cells [17,18]. Its involvement in

Abbreviations: cADPR, cyclic adenosine diphosphate ribose; DBU, 1,8-diazabicyclo[5.4.0]undec-7-ene; DBCO, dibenzocyclooctyne; DCM, dichloromethane; DEAE, diethylaminoethyl-; HRMS, high resolution mass spectrometry; IP3, inositol 14,5-trisphosphate; NAADP, nicotinic acid adenine dinucleotide phosphate; PEG, polyethyleneglycol; RyR, ryanodine receptor; SAR, structure activity relationship; SAA, streptavadin-agarose; *t*-BuONO, *tert*-butyl nitrite; TFA, trifluoroacetic acid; THF, tetrahydrofuran; THPTA, tris(benzyltriazolylmethyl)amine; TMS-N_3, azidotrimethylsilane; TPC, two pore channel; TRP-ML1, transient receptor potential cation channel, mucolipin subfamily 1; WCL, whole cell lysate

* Corresponding author at: Department of Medicinal and Biological Chemistry, University of Toledo, Toledo, OH, 34614, United States.
** Corresponding author at: Department of Pharmacology, University of Minnesota Medical School, Minneapolis, MN, 55455, United States.
E-mail addresses: walse001@umn.edu (T.F. Walseth), james.slama@utoledo.edu (J.T. Slama).

https://doi.org/10.1016/j.ceca.2019.102060
Received 16 May 2019; Received in revised form 11 July 2019; Accepted 15 July 2019
Available online 01 August 2019
0143-4160/

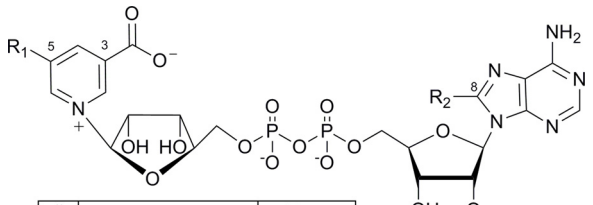

#	R_1 =	R_2 =
1	-H	-H
2	$-N_3$	-H
3	$-(CH_2)_3$-NH-*t*-Boc	-H
9	$-N_3$	$-C\equiv C-H$

Fig. 1. Structure of nicotinic acid adenine dinucleotide phosphate (NAADP, **1**), the photoaffinity label 5-azido-NAADP (**2**), 5-(3-(*t*-Boc-amino)-propyl)-NAADP (**3**), and 5-azido-8-ethynyl-NAADP (**9**).

immunity, where NAADP signaling regulates T cell motility and reactivation, has been observed [19–21].

NAADP was first synthesized using the pyridine base-exchange activity of NAD glycohydrolase (CD38) or *Aplysia californica* ADP-ribosyl cyclase [22,23]. In this procedure, NADP is treated with the enzyme in the presence of high (millimolar) concentrations of an added pyridine base (Fig. 2). The enzyme catalyst cleaves the pyridinium-ribose bond forming an ADP-ribosyl-enzyme intermediate which subsequently reacts with the added pyridine base, resulting in the formation of a pyridine-substituted NADP analog. In the presence of nicotinic acid and at low pH, formation of useful quantities of NAADP is the result. *Aplysia californica* ADP-ribosyl cyclase is a member of this family of enzymes that catalyze the pyridine base-exchange reaction, is available as a soluble recombinant protein, and is stable to storage and the conditions of the enzymatic reaction [24]. This enzyme-catalyzed base-exchange reaction has allowed us and others to produce NAADP analogs with substitution on the nicotinic acid moiety [25–28].

The intracellular Ca^{2+} stores targeted by NAADP are different from those regulated by IP3 or cADPR [29,30]. NAADP-sensitive Ca^{2+} stores reside in acidic compartments termed reserve granules (in sea urchin eggs) or lysosome-like and endosome-like acidic vesicles (in mammalian cells). The identity of the ion channel(s) regulated by NAADP remains controversial. The prime candidates are the two pore channel (TPC) family [9,31], although other targets have been implicated including the type 1 ryanodine receptor (RyR1) [32] and the transient receptor potential mucolipin 1 channel (TRP-ML1) [33].

NAADP-evoked Ca^{2+} release likely occurs through engagement of NAADP binding proteins (NAADP receptor) that associate with these Ca^{2+} permeable ion channels. These NAADP binding proteins were first implicated using [^{32}P]-5-N_3–NAADP (**2**) (Fig. 1) as a photoaffinity label to determine the number and the molecular weights of NAADP binding proteins in sea urchin egg homogenates [34] and in mammalian cell extracts [35,36]. Remarkably, the photoprobe selectively labeled relatively low molecular weight proteins differing from TPCs [34] as well as from the other ion channels proposed to be regulated by NAADP [35]. In sea urchin egg extracts, irradiation of low concentrations of [^{32}P]-5-N_3-NAADP was shown to specifically label proteins with molecular weights of 45, 40 and 30 kDa, whereas in cultured mammalian cells a ~23 kDa protein doublet was specifically labeled. Labeling of NAADP binding proteins was preserved in pancreatic extracts of TPC1 and TPC2 knock-out mice [35], further indicating that the labeled proteins did not represent either TPC or TPC proteolytic fragments. Lin-Moshier et al. further demonstrated that although NAADP binding was enhanced in HEK 293 cells overexpressing recombinant TPC, enhanced binding was disproportionally low when compared to the expected increase in the number of copies of the TPC [35].

Our photoaffinity labeling studies therefore suggested that NAADP was bound to a novel receptor protein, and that this protein likely controlled one or more Ca^{2+} selective ion-channels through protein-protein interaction [35]. The NAADP binding protein has not been identified, and therefore the mechanism of NAADP-evoked Ca^{2+} mobilization remains unclear. The isolation and characterization of the NAADP binding protein will provide invaluable information on understanding the Ca^{2+} signaling mechanism involved.

To achieve this goal, we sought a bi-functional NAADP analog that contained an aryl azide group which, on irradiation, would covalently crosslink adjacent amino acid residues within a binding site through a photochemical reaction. A second functional group was envisioned which could subsequently react through a “click chemistry” reaction with a fluorescent label or an affinity tag for subsequent isolation of the photo-crosslinked receptor protein. Previous studies on the structure activity relation (SAR) of NAADP analogs using sea urchin egg homogenates suggested that a relatively large substituent could be attached to the nicotinic acid 5-position while still retaining agonist activity and high binding affinity [28]. We had previously synthesized and tested 5-(3-(*t*-Boc-amino)-propyl)-NAADP (**3**, Fig. 1), and found that it was an agonist with an EC_{50} in the micromolar range. On this basis we proposed to synthesize substituted nicotinic acid **4**, exchange it into NAADP using enzyme catalyzed base-exchange, and produce bifunctional “all-in-one-clickable” NAADP (AIOC-NAADP, **5**) (Fig. 3). AIOC-NAADP (**5**) is equipped with both a photoactive aryl azide and a “clickable” aliphatic azide. Similar bi-substituted benzyl groups and bi-substituted benzoic acid groups had been synthesized recently, and used as “clickable” photoaffinity labels in the study of receptors and enzymes [37–40]. In this work have characterized AIOC-NAADP, **5,** determined its ability to trigger NAADP mediated Ca^{+2} release, and showed in cultured mammalian cells that it photolabels the same proteins that were detected using photoaffinity label **2**.

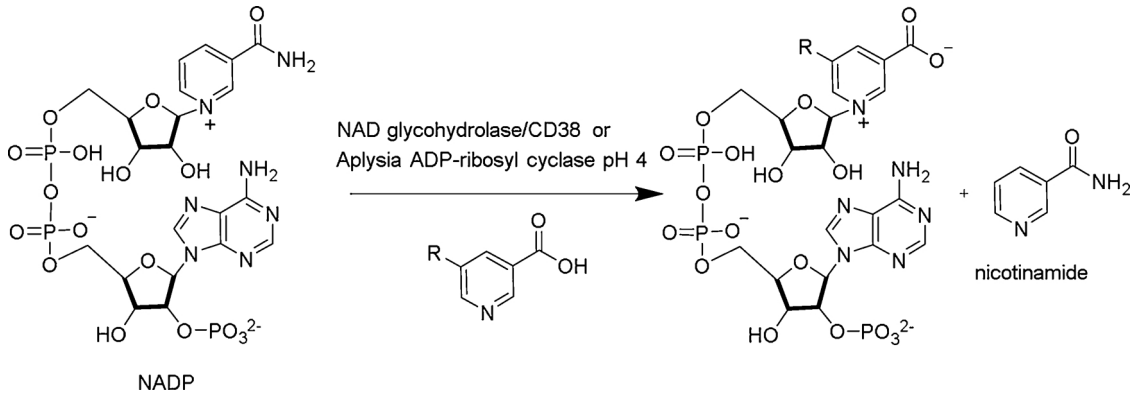

Fig. 2. Pyridine base exchange reaction catalyzed by NAD glycohydrolase (CD38) or *Aplysia californica* ADP-ribosyl cyclase using NADP and nicotinic acid or a substituted nicotinic acid as co-substrates.

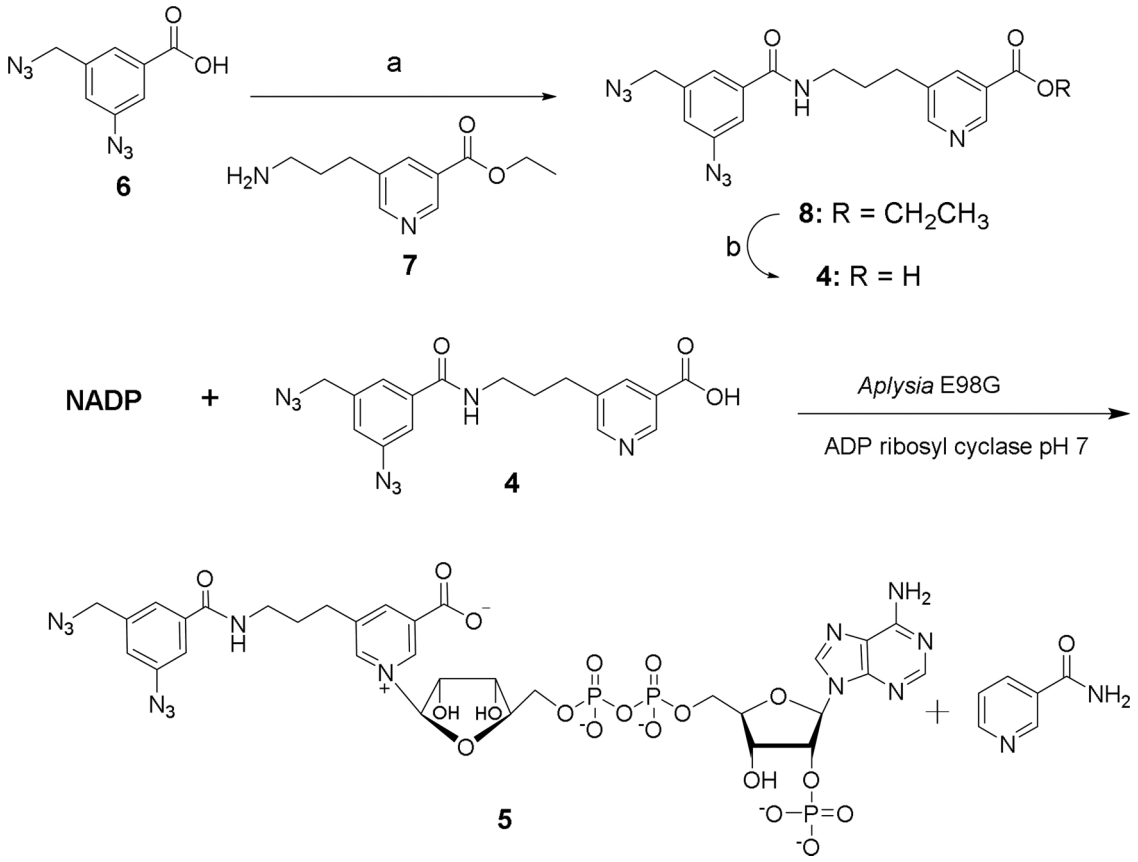

Fig. 3. Synthesis of the AIOC-NAADP analog **5** from NADP and bifunctional nicotinic acid analog **4** using recombinant E98 G *Aplysia californica* ADP-ribosyl cyclase catalyzed base exchange reaction. Reagents and conditions: (a) N-hydroxysuccinimide, N,N′-diisopropylcarbodiimide, DIPEA, THF, RT, 16 h, 63.5% (b)(i) 4 N KOH, 4 h, THF − CH_3OH (1:1); (ii) 1 M aq. HCl, 60.1%.

2. Results

2.1. Synthesis of AIOC-NAADP required nicotinic acid 4 and NADP

The strategy for production of the AIOC-NAADP (**5**) required the synthesis of the pyridine base **4** from **6** and **7** (Fig. 3). The synthesis of **6** [39] and **7** [28] have both been described, and our modifications of the procedures are detailed in Supporting Information Fig. S-1. Compounds **6** and **7** were coupled using carbodiimide, resulting in the formation of amide **8**, which was hydrolyzed yielding pyridine base **4** (Fig. 3).

2.2. Enzyme catalyzed base exchange converted NADP and 4to AIOC-NAADP (5)

Synthesis of NAADP analog **5** was initially attempted using the enzyme catalyzed base exchange reaction with *Aplysia californica* ADP-ribosyl cyclase, the pyridine base **4**, and NADP. A 10–20 eq. of pyridine base was reacted with 1 eq. of NADP in aqueous buffer at pH 4 as illustrated in Fig. 3 [23]. The pyridine base exchange with the wild type enzyme requires that the pyridine carboxylic acid be protonated and neutral and this in turn requires that the exchange reaction be carried out at a pH of about 4.5. We found that compound **4** was an inefficient substrate for the base-exchange reaction under these conditions, likely because of its low solubility in buffered water at pH 4.5, limiting the concentration that could be achieved and preventing the base-exchange reaction from occurring in high yield. At higher pH (pH $\geq$ 5), compound **4** was completely soluble. In an investigation by Graeff et al., X-ray crystallography and site directed mutagenesis studies performed on wild type *Aplysia californica* ADP-ribosyl cyclase had established the presence of an acidic Glu^{98} residue in the active site [41]. At a high pH, electrostatic repulsion between the Glu^{98} carboxylate and the ionized carboxylate of nicotinic acid prevented the binding and the exchange of the nicotinate anion. The base-exchange reaction using a nicotinic acid derivative therefore could only occur at a low pH at which the nicotinic acid was neutral. We altered the reaction conditions and utilized a mutant homolog of *Aplysia* cyclase, E98 G. E98 G has one of the acidic residues, Glu^{98}, replaced by a neutral glycine and this eliminates the electrostatic repulsion that could be created in the presence of the pyridine base at a higher pH [42]. As a result, the base-exchange reaction was run at a pH of 7, using 18 eq. of compound **4**, 1 eq. of NADP, at 37 °C yielding the AIOC-NAADP (**5**) in an isolated yield of 35%.

2.3. Spectroscopic properties of AIOC-NAADP (5)

Following anion exchange purification AIOC-NAADP (**5**) was shown to be a single component by HPLC and its structure was confirmed by ^{1}H-NMR, ^{31}P-NMR and high resolution mass spectrometry (see 4. Experimental Procedures). The electronic absorption spectrum of **5** at neutral pH exhibits a maximum at 253 nm (Fig. 4). As compound **5** is irradiated for 1–3 min using a hand-held short wave ultraviolet emitting mineral light, the λ_{max} was observed to shift to a longer wavelength at 257.5 nm and the intensity of the absorption decreases. A long wavelength tail with absorption between 320–380 nm also appears on irradiation (Fig. 4). Irradiation for more than 3 min did not elicit any further changes in the UV spectra. The observed changes in the absorption spectra support the presence of an arylazide which upon irradiation is predicted to lose N_2 and produce an electrophilic photoproduct that can react with solvent water.

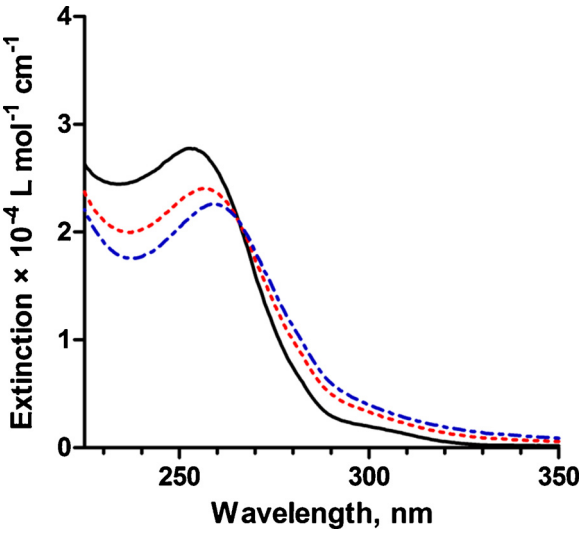

Fig. 4. UV spectrum of AIOC-NAADP (**5**)(solid black line) and spectra following the irradiation of **5** with short wavelength UV light for 1 min (dotted red line) and 3 min (dashed and dotted blue line). Additional irradiation produced no further changes. All of the spectra were obtained in 20 mM HEPES at pH 5.

2.4. Recognition of AIOC-NAADP (5) by mammalian and sea urchin egg NAADP receptors

The ability of AIOC-NAADP to elicit calcium release was examined in two biological systems. The first system utilized microinjection of intact SKBR3 cells transfected with TPC2 and the fluorescent calcium indicator protein GCaMP6M [43,44]. These transfected SKBR3 cells are large and adherent cells which can be microinjected. They respond robustly to microinjected NAADP with increased fluorescence without requiring the addition of a Ca^{2+} sensitive fluorescent dye. Fig. 5 shows that microinjection of either NAADP (**1**) or AIOC-NAADP (**5**) into single SKBR3 cells resulted in a concentration dependent cytoplasmic fluorescent calcium signal, while buffer injection was without effect. Quantitation of the effects of microinjection are depicted in Fig. 5 Panel A and B. Plotting the fold-change in the intensity of the Ca^{2+} signal verses the concentration of **1** or **5** in the micropipette showed saturation of the response characterized by an EC_{50} of 22 nM for NAADP and an EC_{50} of 173 nM for AIOC-NAADP (Fig. 5 Panel D). Microinjection of either NAADP (**1**) or AIOC-NAADP (**5**) into SKBR3 cells with endogenous levels of TPC2 expression also mobilized intracellular calcium stores, an effect which could be blocked by depleting lysosomal calcium content using the vacuolar-ATPase inhibitor, bafilomycin A1 (Fig. 5 Panels E and F). The bafilomycin results are similar to those obtained in SKBR3 cells overexpressing TPC1 [43]. The magnitude of the peak calcium responses evoked by NAADP or AIOC-NAADP was approximately 5-fold higher in cells transiently expressing TPC2 compared to non-transfected cells.

The second system employed sea urchin egg homogenates, an *in vitro* system with well characterized NAADP responses [45,46]. The pharmacological properties of AIOC-NAADP (**5**) were characterized for Ca^{2+} release and for binding. We found that the NAADP analog **5** was poorly recognized by the sea urchin NAADP receptor. Fig. 5 Panel G shows that compound **5** did not elicit release of Ca^{2+} from sea urchin egg homogenates at concentrations less than 100 μM, but did release a small amount of calcium at 1 mM (18% of the amount of calcium released by a 10 μM NAADP (**1**)). A unique feature of the sea urchin egg extract system is a self-inactivation/desensitization process by which NAADP-induced calcium release can by inactivated by subthreshold concentrations of NAADP in a time- and concentration-dependent manner [47,48]. Pre-incubation of sea urchin egg extract with varying concentrations of AIOC-NAADP (**5**) for seven minutes followed by addition of 1 μM NAADP produces a concentration-dependent decrease (desensitization) in the ability of 1 μM NAADP to release calcium (Fig. 5H, filled circles). The IC_{50} for AIOC-NAADP (**5**) desensitization was 13 μM, whereas NAADP (**1**) produced desensitization with an IC_{50} of 0.3 nM (data not shown). Fig. 5 Panel H, open circles, also shows that AIOC-NAADP (**5**) competes with [^{32}P]-NAADP in a competition-binding assay in sea urchin egg extracts with an IC_{50} of 6 μM. Overall, the data in Fig. 5 suggests that AIOC-NAADP is a potent agonist in the SKBR3 system, but not very potent in the sea urchin egg system.

2.5. Specific photolabeling of NAADP binding proteins using [^{32}P]-5

Next we determined if [^{32}P]-labeled AIOC-NAADP ([^{32}P]-**5**) would label the same intracellular targets that were detected in our previous studies using [^{32}P]-5-N_3-NAADP (**2**) [34–36]. We first showed that [^{32}P]-AIOC-NAADP (**5**) would specifically label 23–24 kDa protein(s) in SKBR3 cells (Fig. 6 Panel A). NAADP mediated signaling has been extensively characterized in both SKBR3 and in Jurkat cells both in terms of calcium mobilization [20,35,43,49–51] and photolabeling of NAADP binding proteins [20,36]. Jurkat cells were one of the first mammalian systems shown to be responsive to NAADP [49], and subsequently Jurkat cells were shown to mobilize intracellular NAADP in response to activation of the cell surface T cell receptor [49,52]. This functional response motivated us to characterize the photolabeling of Jurkat cell extracts with **5**, even though we did not possess the technology that would enable us to study Jurkat cells by microinjection.

The results of this photoaffinity labeling study are shown in Fig. 6 Panel B. When Jurkat cell extracts were irradiated in the presence of low concentrations (~1 nM) of [^{32}P]-5-N_3-NAADP or [^{32}P]-**5**, we observed labeling of multiple protein bands (Fig. 6B). The labeling patterns with both probes were qualitatively similar, however, ([^{32}P]-**5**), produced more intense labeling of most of the bands compared to [^{32}P]-5-N_3-NAADP (**2**). No photolabeling of the Jurkat extract was observed without irradiation (see Supporting Information Fig. S-2). When unlabeled 1 μM NAADP was included, only a 23 kDa protein labeled by both probes was protected from photoderivatization. This indicates that [^{32}P]-5-N_3-NAADP (**2**), [^{32}P]-**5** and NAADP (**1**) compete for a common binding site, and identifies the 23 kDa protein as a specifically labeled protein. A specifically labeled band at 23 kDa was also observed in SKBR3 cell extracts (Fig. 6A), the system we used to demonstrate that AIOC-NAADP (**5**) was active in mammalian systems in Fig. 5. This photolabeling data is consistent with our published data using [^{32}P]-5-N_3-NAADP (**2**) in SKBR3 and Jurkat cell extracts [35,36]. The time course of [^{32}P]-**5** labeling is shown in Supporting Information Fig. S-2. The labeling of the 23 kDa protein was detected within 15 s and increased rapidly during the first 15 min of preincubation prior to irradiation. The labeling then plateaued.

Fig. 6 Panel C shows a similar photolabeling system comparing [^{32}P]-5-N_3-NAADP (**2**) and [^{32}P]-**5** using sea urchin egg (*S. purpuratus*) extracts. Neither probe labeled any proteins in the absence of UV irradiation. Irradiation in the presence of [^{32}P]-5-N_3-NAADP (**2**) produced labeled proteins with molecular weights of 45, 40 and 30 kDa. The photolabeling of these proteins was protected by the inclusion of 1 μM NAADP, data that is consistent with our previously published data [34]. Irradiation in the presence of [^{32}P]-**5** resulted in the labeling of several additional proteins, however, the labeling of these proteins was non-specific as the inclusion of 1 μM NAADP did not protect the labeling of any of these bands.

The selectivity of photolableing of the 23 kDa protein by [^{32}P]-**5** was evaluated by examining the labeling in the absence and presence of increasing concentrations of NAADP (**1**), NADP and AIOC-NAADP (**5**). Fig. 7A and B show the labeling patterns of Jurkat cell extracts labeled with [^{32}P]-**5** in the presence of increasing concentrations of NAADP and NADP (Fig. 7A) or AIOC-NAADP (**5**) (Fig. 7B). Fig. 7C compares the intensity of the 23 kDa labeled band, as measured by densitometry of the phosphorimage, as concentrations of the competing ligand were

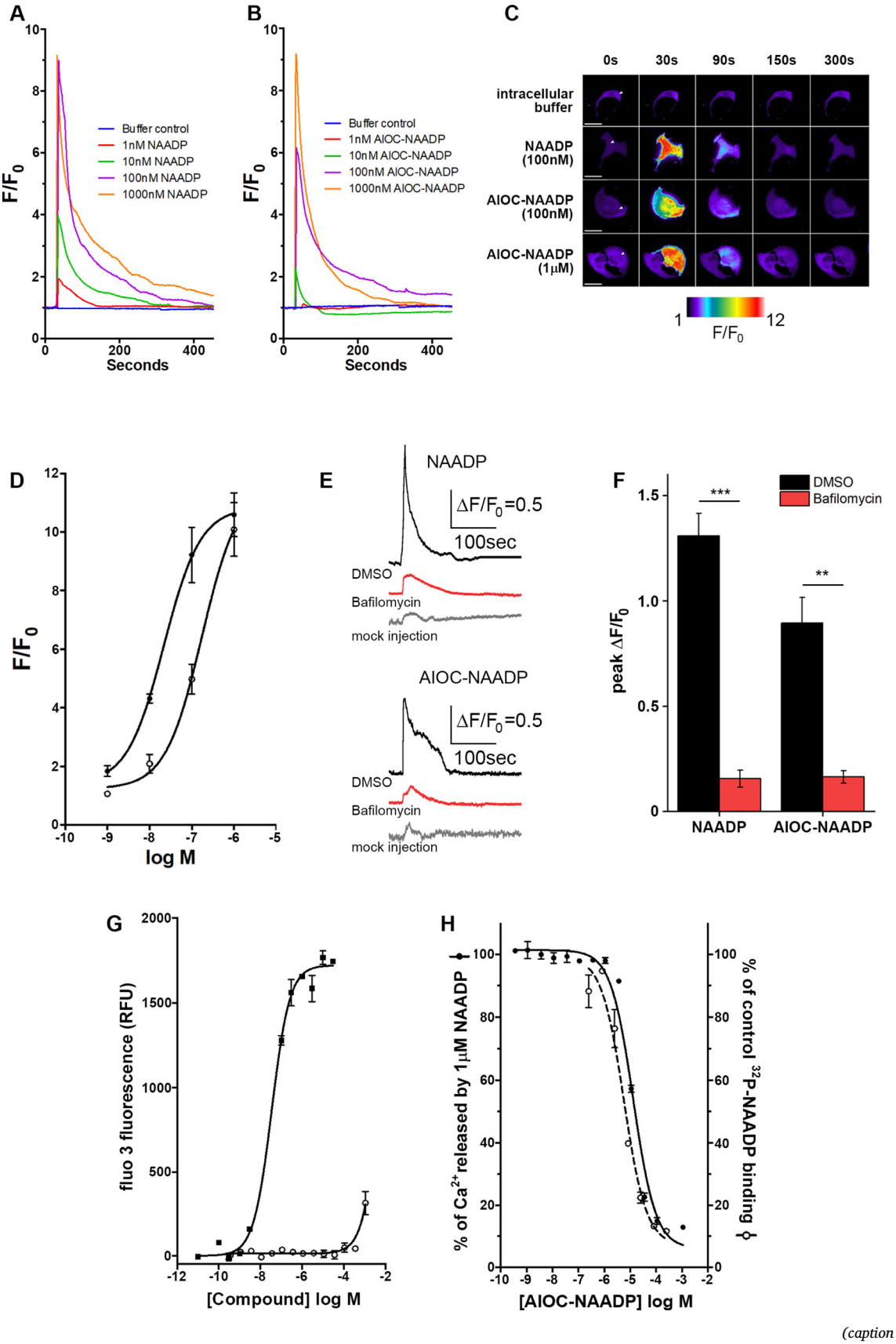

(caption on next page)

varied. NAADP protected the 23 kDa band from photolabeling most potently (IC_{50} = 20 nM), whereas 40-fold higher concentrations of NADP (IC_{50} = 795 nM) were required to achieve similar levels of protection. AIOC-NAADP (**5**) prevented labeling with an IC_{50} of 100 nM, a value in reasonable agreement with that measured from micoinjection studies.

Fig. 5. AIOC-NAADP induces calcium mobilization in SKBR3 cells and sea urchin egg homogenates. SKBR3 cells transiently overexpressing TPC2-mRuby2 were microinjected with varying concentrations NAADP (Panel A) or AIOC-NAADP (Panel B). Concentrations refer to pipette concentrations. Pseudocolored images of GCaMP6M fluorescence intensity in response to microinjection of the indicated compounds is shown in Panel C, white arrowheads indicate injection sites, scale bars represent 10 μm. Panel D shows the concentration dependence curves for NAADP (solid circles) and AIOC-NAADP (open circles). All data n = 3, except the 100 nM data which is an n = 4. Panel E shows representative GCaMP6M fluorescence traces from SKBR3 cells with endogenous TPC2 expression after microinjection with NAADP (100 nM, top) or AIOC-NAADP (1μM, bottom) after 30 min incubation with DMSO (0.1%, black) or bafilomycin A1 (100 nM, red). Mock injections (intracellular buffer, grey) responses are shown for comparison. Quantification of the cumulative dataset of injections in SKBR3 cells with endogenous TPC2 expression is shown in panel F, all data are n = 3, **p < 0.01, ***p < 0.001 using the student's t-test. Panel G shows the concentration dependence of NAADP (closed circles) and AIOC-NAADP on calcium release from sea urchin egg homogenates. Panel H shows the ability of AIOC-NAADP to produce desensitization of the ability of 1 μM NAADP to release calcium homogenate (solid circles) and compete with ^{32}P-NAADP in a competition-binding assay (open circles). Both sets of data were performed in sea urchin egg homogenates and data represent an n = 3).

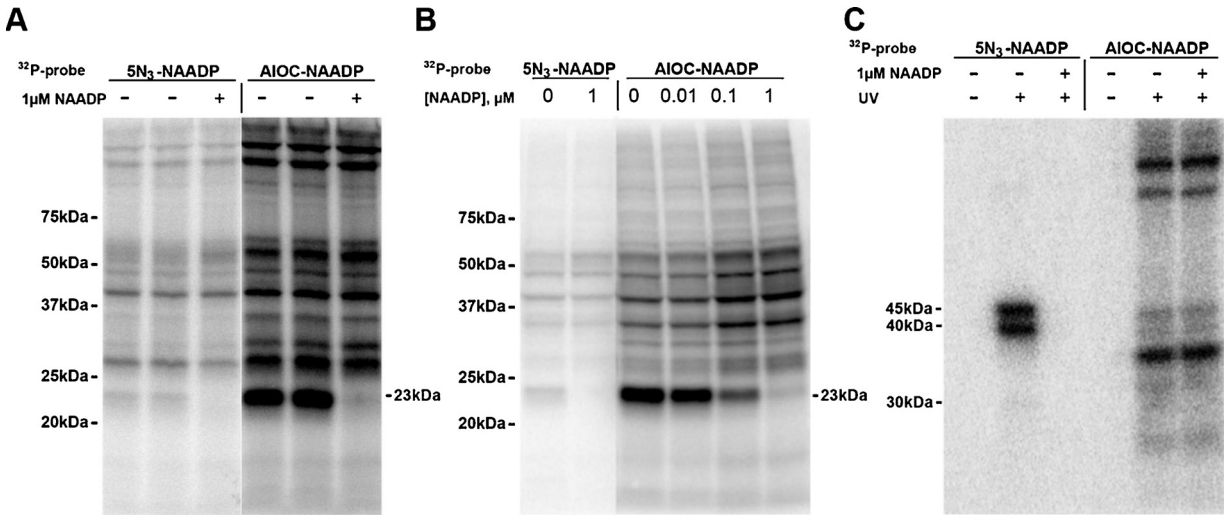

Fig. 6. Comparison of [^{32}P]-AIOC-NAADP and [^{32}P]-5-N_3-NAADP photolabeling in SKBR3 cell extracts (Panel A), Jurkat cell extracts (Panel B), and sea urchin egg extracts (Panel C). SKBR3 (A) or Jurkat (B) cell extracts were photolabeled with either [^{32}P]-AIOC-NAADP (1.2 nM) or [^{32}P]-5N_3-NAADP (0.5 nM) in the absence or presence of the indicated concentrations of unlabeled NAADP. Panel C: Sea urchin egg homogenates were photoaffinity labeled with [^{32}P]-AIOC-NAADP (1 nM) or [^{32}P]-5N_3-NAADP (0.4 nM). The probe used, irradiation conditions and the presence of unlabeled NAADP are indicated.

Since our previous photoaffinity labeling studies relied on [^{32}P]-5-N_3-NAADP (**2**), we wanted to carefully demonstrate that the labeling of the 23–24 kDa proteins would show cross competition with 5-N_3-NAADP (**2**) and AIOC-NAADP (**5**) as predicted for probes which label the same protein through a common binding site. This is demonstrated in Fig. 8, where labeling of the 23 kDa proteins with [^{32}P]-5-N_3-NAADP (**2**) was protected by both NAADP and AIOC-NAADP. We also note that in Fig. 8 an approximately 45 kDa protein was labeled by 5-N_3-NAADP (**2**) and protected in the presence of low concentrations of NAADP but poorly protected by AIOC-NAADP. It additionally appears that a 25 kDa protein is labeled by [^{32}P]-5-N_3-NAADP (**2**) and partially protected by NAADP and AIOC-NAADP, indicating a further diversity of NAADP binding proteins.

Fig. 9 shows the dependence of [^{32}P]-labeled AIOC-NAADP ([^{32}P]-**5**) photolabeling on the concentration of [^{32}P]-labeled AIOC-NAADP. Fig. 9 Panel A shows the intensity of labeling of all bands increases as a function of the concentration of [^{32}P]-labeled AIOC-NAADP. Only the labeling of the 23 kDa band was labeled specifically as inclusion of unlabeled 2.5 μM NAADP prevented the labeling. A 32 kDa band was partially protected by the 2.5 μM NAADP. The labeling of this band was also partially protected by 1 μM NAADP and NADP (see Fig. 7A). Fig. 9 Panel B shows the saturation of the 23 kDa labeling by [^{32}P]-labeled AIOC-NAADP ([^{32}P]-**5**). Specific photolabeling of the 23 kDa protein was determined by densitometric analyses of the data shown in Fig. 9A

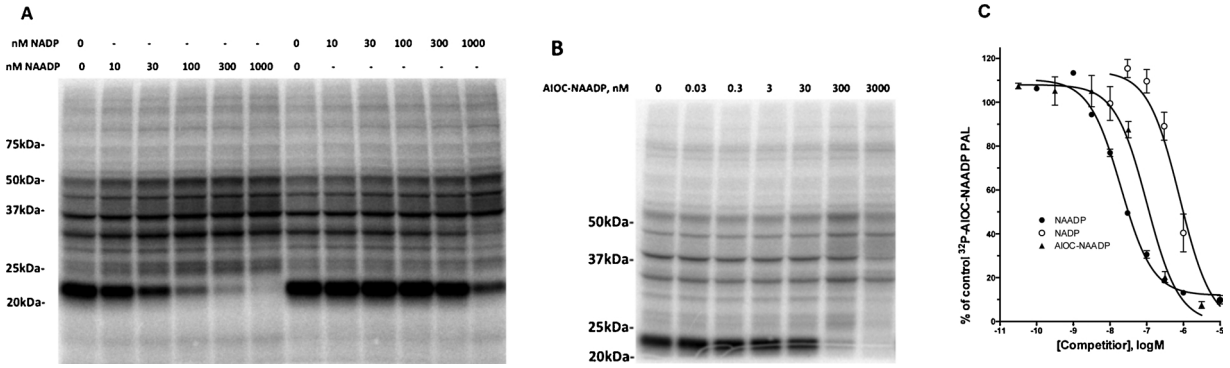

Fig. 7. Specificity of [^{32}P]-AIOC-NAADP photolabeling in Jurkat cell extracts. Panel A. Phosphorimage of a gel examining the effect of NAADP and NADP on [^{32}P]-AIOC-NAADP (0.3 nM) photolabeling. Panel B. Phosphorimage of a gel examining the effect of AIOC-NAADP on [^{32}P]-AIOC-NAADP photolabeling. Photolabeling was performed with Jurkat cell extracts in the absence or presence of the indicated concentrations of unlabeled NAADP or NADP or AIOC-NAADP. Panel C. Densitometric analyses of experiments similar to those shown in Panels A and B (n = 3).

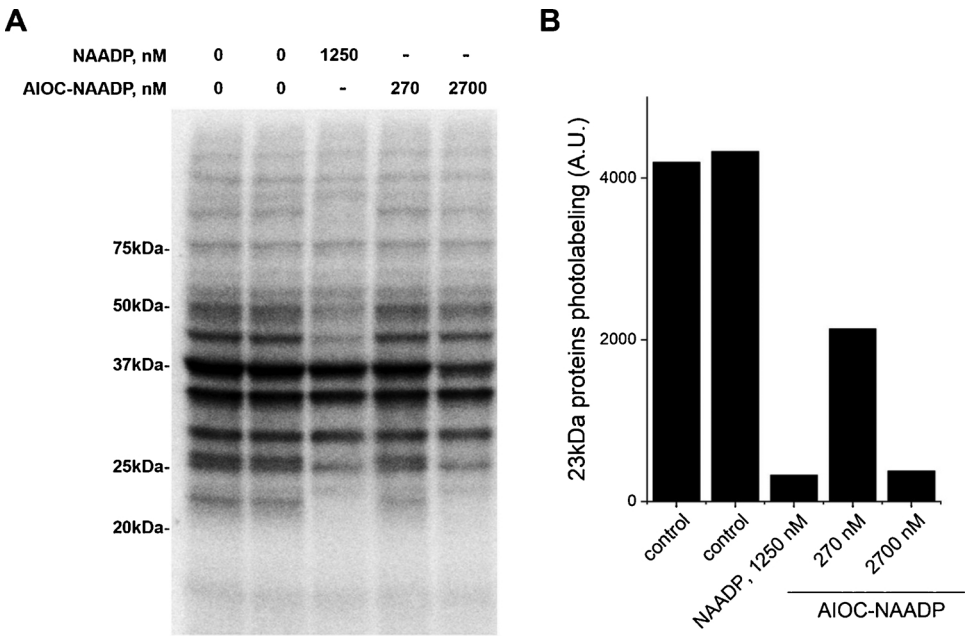

Fig. 8. Displacement of [^{32}P]-5-N_3-NAADP with AIOC-NAADP. Panel A: Phosphorimage of Jurkat cell extracts photolabeled with 6 nM [^{32}P]-5N_3-NAADP in the absence or presence of the indicated concentrations of NAADP or AIOC-NAADP. Panel B: Densitometry analysis of photolabeling of 23 kDa proteins.

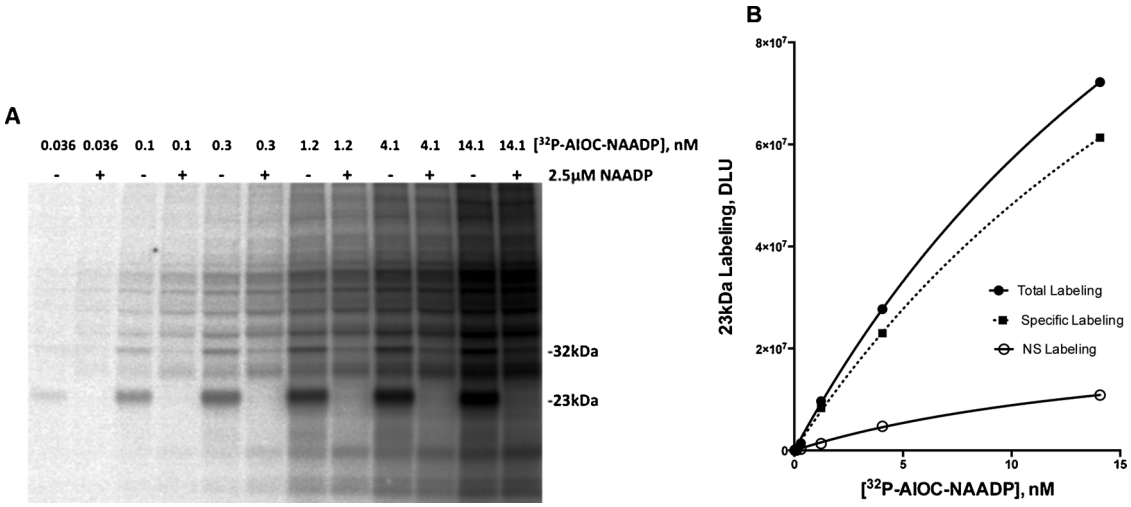

Fig. 9. Photolabeling of Jurkat cell extracts with increasing concentrations [^{32}P]-AIOC-NAADP. Panel A. Photolabeling of Jurkat cell extracts with increasing concentrations of [^{32}P]-AIOC-NAADP in the absence (-) and presence (+) of 2.5 μM NAADP. A phosphorimage of the gel is shown. Panel B. Saturation of the [^{32}P]-AIOC-NAADP photolabeling of the 23 kDa band. Total labeling (closed circles), non-specific labeling (open circles) and specific labeling (closed square/dashed line) of the 23 kDa band were determined by densitometric analyses of the phosphorimage.

(specific labeling is the difference between the labeling in the absence (total labeling) and presence of 2.5 μM NAADP (non-specific labeling). Although we were unable to achieve concentrations of [^{32}P]-labeled AIOC-NAADP that saturated the labeling, the K_d value of AIOC-NAADP (**5**) estimated from non-linear regression analysis of the specific labeling curve of Fig. 9B was 28 nM. This is consistent with the functional data in Fig. 5D and photolabeling data in Fig. 7C that AIOC-NAADP (**5**) is a high affinity probe for NAADP binding sites in mammalian systems.

2.6. Proteins photolabeled with [^{32}P]AIOC-NAADP were biotinylated using "click chemistry" and affinity isolated

We next tested whether the proteins photolabeled by the bifunctional probes could be reacted with reagents containing a biotin affinity tag through "click chemistry". Fig. 10 shows the data for probe **5**. Jurkat cell extracts were photoaffinity labeled with [^{32}P]-labeled probe **5**. After removal of the free probe, the sample was subjected to click reaction with four different reagents using either copper (I) catalyzed click chemistry or strain promoted click chemistry using dibenzyl cyclooctyne (DBCO) reagents. The biotin reagents contained either PEG or diazo based linkers between the biotin affinity tag and the clickable moieties (alkyne for Cu (I) catalyzed reactions and DBCO for strain promoted click chemistry). The control for these experiments consisted of a Jurkat cell extract that had been photolabeled with [^{32}P]-labeled probe **5**, but not subjected to click chemistry. After the click reaction, the excess reagents were removed by desalting and the extracts were incubated with streptavidin-agarose beads to absorb the biotinylated proteins. The streptavidin-agarose beads were washed 5-times with phosphate buffered saline to remove proteins bound non-specifically to the beads. Proteins specifically bound to the beads at this point were removed by boiling the beads in 2× Laemmli SDS sample buffer for 10 min. The eluted proteins were examined by SDS-PAGE and

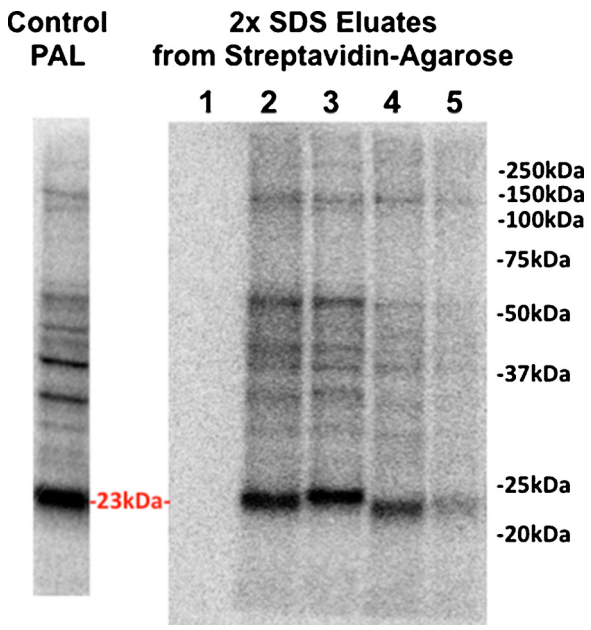

Fig. 10. Proteins photolabeled by bifunctional probe **5** can be biotinylated *via* click chemistry and recovered using streptavidin-agarose. Human Jurkat cell extract was photoaffinity labeled with 0.3 nM [^{32}P]-AIOC-NAADP (**5**) and divided into five equal aliquots. One aliquot served as a control, while the other four were subjected to click chemistry with various biotin containing click chemistry reagents. After click chemistry, all aliquots were incubated with streptavidin-agarose for 12 h and the beads were subsequently washed with PBS, to remove non-specifically bound proteins. Proteins bound at this point to the beads were eluted by boiling the washed beads in 2 × SDS sample buffer for 10 min. The eluted proteins were run on a SDS-PAGE gel which was dried and exposed to a phosphor image screen for 24 h. The far left lane labeled Control PAL represents the pattern of photolabeling obtained in the original sample (note: this sample was run on a different gel than the samples eluted from the beads). Lane 1: control sample that was not subjected to click chemistry; Lane 2: click chemistry with dibenzylcyclooctyne(DBCO)-diazo-linked biotin; lane 3: click chemistry with DBCO-PEG-linked biotin; lane 4: Cu(I) click chemistry with alkyne-diazo-linked biotin; lane 5: Cu(I) click chemistry with alkyne-PEG-linked biotin. Note that radiolabeled proteins were only recovered from the streptavidin-agarose beads when the photoaffinity labeled sample was subjected to click chemistry. No labeled proteins were recovered in the control sample (lane 1) that was photoaffinity labeled but not subjected to click chemistry with a biotin reagent. In addition, the 23 kDa protein that we have shown to be specifically labeled with probe **5** is recovered from all the samples subjected to click chemistry (lanes 2–5).

radiolabeled proteins were detected using a phosphorimager. Fig. 10 shows that [^{32}P]-labeled proteins were eluted from each of the samples subjected to click reaction. No labeled proteins were detected in the control sample that had been photolabeled with **5**, but not subjected to click reaction (Fig. 10, lane 1). Noteworthy, the 23 kDa protein that we have shown to be specifically labeled with probe **5** is recovered from all the samples subjected to click chemistry (Fig. 10, lanes 2–5). This demonstrates that probe **5** is "clickable" after photo-incorporation of the probe into the protein. Based on the radioactivity recovered from the streptavidin-agarose beads, we estimated that the click reagents derivatized between 15 and 30% of the labeled proteins depending on which biotin reagent and click reaction was employed. The best results were with a DBCO PEG-linked biotin. What is not apparent from the radiometric detection is that a high background of biotinylated proteins due to the non-specific reaction of the biotinylated-acetylenes was encountered in every case. This non-specific reactivity that accompanies the click reactions had been observed previously [53,54]. In the present case, the non-specificity must be overcome before identification of labeled proteins by mass spectrometry or Edman degradation will be possible. Optimizing click-reaction conditions are expected to increase the efficiency of the click chemistry reactions and to decrease non-specific background.

3. Discussion

AIOC-NAADP (**5**) was designed as a bifunctional NAADP analog that would specifically photolabel and subsequently facilitate the pull-down of NAADP binding proteins. Its synthesis represents an extension of our previously published enzymatic methodology for producing NAADP analogs, in that we have shown that the *Aplysia californica* ADP-ribosyl cyclase E98 G mutant can be used for the production of analogs from hydrophobic nicotinic acid bases that would otherwise fail when using wild type enzyme as the catalyst [28].

Analog **5** was shown to be recognized at low concentration by the human NAADP receptor, but in contrast in sea urchin egg homogenates, **5** was found to be a poor low potency agonist, although it produced sub-threshold desensitization in the low micromolar range. Consistent with these differential potencies at evoking Ca^{2+} release in the human and sea urchin system, **5** showed strong, specific labeling of the 23 kDa NAADP binding protein(s) in different immortalized human cell lines, but no specific labelling of the previously identified NAADP binding proteins in sea urchin homogenate. Differences in the structure activity relationship between human and the sea urchin NAADP receptors have been observed previously [55], and these data reinforce the relationship between the specifically photolabeled binding proteins and the NAADP-evoked Ca^{2+} release mechanism in both systems.

The key finding is that [^{32}P]-**5** specifically photo-labeled the 23 kDa protein(s) in cultured human cells that we had previously specifically labeled using [^{32}P]-5-N_3–NAADP (**2**) [35,36]. Labeling with [^{32}P]-**5** was shown to saturate at low concentration and [^{32}P]-**5** was demonstrated to compete with both NAADP and 5-N_3-NAADP for a common binding site. Our photolabeling studies with [^{32}P]-**5** indicate that despite the significant difference in structure of NAADP (**1**) and 5-N_3–NAADP (**2**), *versus* AIOC-NAADP (**5**), **5** is capable of specifically recognizing 23 kDa NAADP binding proteins.

Last we demonstrated that the proteins which were photolabeled with [^{32}P]-**5** could be "clicked" to biotinylated acetylene containing labels and the proteins so derivatized isolated by biotin-avidin affinity chromatography. In our brief survey DBCO-biotin was shown to be the most effective, but copper-catalyzed click reaction derivatization was also successful.

This pull-down experiment, was designed to obtain "proof-of-concept", and was therefore performed radiometrically, to provide extremely high sensitivity to detect photo-labeled target proteins even in the presence of non-specific protein background. Indeed, non-specific labeling of proteins was observed, and in the future conditions must be optimized to reduce the background and permit detection of rare targets such as the NAADP binding protein(s).

We have recently described the characterization of another bi-substituted photoaffinity label: 5-azido-8-ethynyl-NAADP (**9**; Fig. 1) [56]. Dinucleotide **9** contains a 5-azide attached to the nicotinic acid ring and an 8-ethyne attached to the purine moiety. Similar to AIOC-NAADP **5**, analog **9** is poorly recognized by sea urchin receptors, but it was active at low concentration when microinjected into cultured human U2OS cells. Our new NAADP analog **5** was shown in this work to be approximately 10-fold more potent than was **9**. Furthermore, at low concentration [^{32}P]-AIOC-NAADP (**5**) consistently produces a more intense labeling, indicative of a higher photoinsertion yield. AIOC-NAADP (**5**) will be most useful for click reactions with biotinylated and dye conjugated acetylenes or with methyl ester-phosphines using the Staudinger ligation reaction. Bifunctional NAADP analog **9** will be applied under circumstances where use of an acetylinic photoprobe followed by a click reaction with a biotinylated azide is desired as a strategy for non-specific click reactivity [53]. Neither **5** nor **9** are well recognized by the sea urchin NAADP receptor, and development of probes specific for the sea urchin receptor remains a priority.

The synthesis of AIOC-NAADP **5** is more straightforward than is the synthesis of **9**, since **5** can be produced directly from enzyme catalyzed base-exchange between NADP and nicotinic acid analog **4**. In contrast, the production of **9** begins with the synthesis of an adenosine nucleoside and requires multiple steps for conversion of the nucleoside into dinucleotide **9**.

The results of this study enable us in future work to use **5** to photoderivatize NAADP binding proteins and subsequently attach them to biotinylated acetylene labels by "click chemistry" for isolation by biotin affinity chromatography. The efficacy of click reactions has been shown to be highly condition dependent [57,58], and future work in applying AIOC-NAADP (**5**) to the identification of NAADP binding proteins will of necessity focus on optimizing the conditions of photoinsertion and for the click reaction to achieve high specificity and low background. Once this is achieved, AIOC-NAADP (**5**) should serve as an effective tool for the labeling and the isolation of NAADP binding proteins in mammalian cells.

4. Experimental procedures

4.1. Biological methods

4.1.1. Plasmids

Plasmid encoding TPC2-mRuby2 was produced by subcloning the TPC2 ORF from previously described plasmid encoding TPC2-myc [59] into pcDNA3-mRuby2 at the NheI restriction site, using standard molecular biology techniques. Plasmids encoding pcDNA3-mRuby2 and GCaMP6M were gifts from Michael Lin and Douglas Kim, respectively (Addgene plasmids, #40260, #40754) [60,61]

4.1.2. Cell culture and transfection

In this study, Jurkat cell extracts are used for most [^{32}P]-AIOC-NAADP photoaffinity labeling experiments (Figs. 6B, 7–9, and Supplementary Fig. S-2) due to the low amount of non-specific labeling present in this cell line - however, photoaffinity labeling of SKBR3 cell extracts is also reported (Fig. 6A). Microinjection of AIOC-NAADP to monitor changes in cytosolic calcium concentrations was conducted in SKBR3 cells as our group is equipped with an injection system that is only suited for adherent cell microinjections, and Jurkat cells are cultured in suspension. Jurkat cells were maintained in RPMI medium, and SKBR3 cells were maintained in McCoy's 5A medium. Cell culture media was supplemented with 10% fetal bovine serum, 100 units/ml penicillin and streptomycin and 292 μg/ml L-glutamine, and cells were cultured at 5% CO_2 and 37 °C. For transfection, SKBR3 cells were seeded in collagen-coated 35 mm glass-bottom dishes (MatTek) at a density of 2×10^5 cells/ml. The following day, cells were transfected with Lipofectamine 2000 according to the vendors protocol. All cell lines were purchased from ATCC. All cell culture and transfection reagents were purchased from Thermo Fisher.

4.1.3. Microinjection and confocal Ca^{2+} imaging

SKBR3 cells were transfected with plasmids encoding TPC2-RFP and GCaMP6M. Dishes were mounted on an Olympus IX81 microscope for imaging. Cells were perfused with Ca^{2+}-free Hank's Balanced Salt Solution (Thermo Fisher) at a rate of 0.5 ml/min. Isolated cells expressing TPC2-RFP and GCaMP6M were identified by fluorescence. Cell morphology was assessed by acquiring z-stack images and reconstructing three-dimensional models of each cell to be injected. Regions that were not relatively close to either the nucleus or the cell periphery were targeted for injection sites. Femtotip (Eppendorf) injection pipettes were backfilled with intracellular buffer (110 mM KCl, 10 mM NaCl, 20 mM HEPES, pH 7.2) containing either vehicle or drug, and were positioned using an Injectman-4 (Eppendorf) micromanipulation system. Cells were injected at a z-position that was approximately 70% of the cell thickness at the site of injection using a Femtojet4i (Eppendorf). Injection parameters were 85 hPa injection pressure, 40 hPa compensation pressure, 0.5 s injection duration, 45° injection angle, and 600 μm/s injection speed. Cells to be injected were imaged (λ_{ex} 488 nm, λ_{em} 514 ± 15 nm bandpass) using a Plan-Apochromat 60x/1.42 oil differential interference contrast objective, and fluorescence changes were monitored using a Yokogawa spinning disk confocal (CSU-X-M1N), and an Andor iXon Ultra 888 EMCCD camera. Image acquisition and data collection was done using Metamorph version 7.10.

4.1.4. Ca^{2+} release, competition ligand binding and sub-threshold desensitization

Studies using the *Strongylocentrotus purpuratus* sea urchin egg homogenate system were performed as described previously [28].

4.2. Chemical methods

4.2.1. General methods

TLC sheets consisting of silica gel layer (200 μm) with a fluorescent indicator coated on a plastic backing were purchased from Baker-flex (Radnor, PA), and were visualized by examination under a 254 nm UV light or sprayed with a 0.5% of ninhydrin (2,2-dihydroxyindane-1,3-dione) dissolved in ethanol solution.

Preparative normal phase and reverse phase purifications were performed using an automated chromatography system equipped with an in-line UV detector (200–360 nm) purchased from Teledyne-Isco (Combiflash R_f system, Lincoln, NE). Pre-packed silica gel columns containing 4 g, 12 g, 40 g, and 80 g of absorbent and reverse phase C-18 columns containing 15.5 g of absorbent were purchased from Teledyne-Isco.

Analytical and large scale anion exchange purifications were performed using a Bio-Rad BioLogic Duoflow HPLC system (Bio-Rad Laboratories, Herculus, CA). Macroporous AG MP-1 anion exchange resin (200–400 mesh, Cl^- form) was purchased from Bio-Rad Laboratories and converted into the trifluoroacetate form according to the manufacturer's instructions. Preparative scale columns used with this resin were packed in an OMNI FIT glass column (1.5 cm × 11.5 cm). A prepacked Bio-Rad Uno-Q anion exchange column (7 × 35 mm) was used for analytical separations. The mobile phase consisted of water and trifluoroacetic acid solution (0–0.1 M). The flow rate, gradient and injection volume was controlled by the unit.

Open column anion exchange purification was performed using diethylaminoethyl (DEAE) cellulose, (DE 53, Whatman Laboratory Products #7153093), packed in a glass Bio-Rad Econo-Column (2.5 cm × 50 cm). The DEAE cellulose resin was conditioned according to the manufacturer's instructions. The flow was controlled using a peristaltic pump (Tris, Teledyne-ISCO, Lincoln, NE) and an automated fraction collector. The mobile phase was ammonium bicarbonate (0–600 mM).

4.2.1.1. Storage and dilution of Aplysia californica ADP-ribosyl cyclase (WT and E98 G) from concentrated aliquots. Recombinant *Aplysia californica* ADP-ribosyl cyclase was produced by the procedure of H. C. Lee et al. [24]. Concentrated solutions of purified WT enzyme were stored at -80 °C at a concentration of 10 mg/ml in 100 μl aliquots. A single 100 μl aliquot of the wild type enzyme was removed from the freezer and thawed in an ice bucket to maintain a temperature of 0 °C. The concentrated aliquot was diluted to 5 ml using 20 mM HEPES buffer (pH = 7.5) to make a final concentration of 0.2 mg/ml. The diluted enzyme solution was mixed thoroughly and transferred into polypropylene plastic vials in 60 μl (12 μg) portions and stored at -80 °C until future use. For the synthesis of NAADP (**1**), three 60 μl portions (36 μg) of the wild type enzyme were utilized for the base exchange of 0.012 mmol of NADP.

Concentrated solutions of purified the mutant E98G *Aplysia californica* ADP-ribosyl cyclase [42] were acquired and stored at −80 °C at concentrations of 0.62 mg/ml and 0.11 mg/ml in 100 μl aliquots. The

concentrated E98 G enzyme was removed from the freezer and thawed in an ice bucket to maintain a temperature of 0 °C and then diluted using 20 mM HEPES (pH = 7.5) to make a final concentration of 0.1 mg/ml. The diluted aliquots were mixed thoroughly and transferred into polypropylene plastic vials in 60 µl (6 µg) portions and stored at -80 °C. For the synthesis of NAADP analog **5**, three or more, 60 µl aliquots of E98 G enzyme (18 µg) were used for the exchange reaction of 0.012 mmol of NADP.

4.2.1.2. HPLC Method 1: analytical anion exchange chromatography. A sample volume of 50 µl of diluted solution (2 mg/ml in nucleotide) was injected onto the 7 mm × 35 mm (1.3 ml) analytical column packed with AG MP-1 resin in trifluoroacetate form. The chromatography was developed at a flow rate of 5 ml/min by applying 10 ml water followed by a linear gradient of 0–45 mM aqueous TFA over a volume of 85 ml. This step was followed by column cleaning and re-equilibration wherein the column was washed with 15 ml of 100 mM aqueous TFA followed by 15 ml deionized water for re-equilibration prior to the next injection.

4.2.1.3. HPLC Method 2: preparative anion-exchange using a shallow gradient. Diluted reaction solution (2 mg/ml in dinucleotide) was loaded into a 5 ml injection loop and loaded onto the 1.5 cm × 11.5 cm column packed with AG MP-1 resin in trifluoroacetate form. The chromatography was developed at a flow rate of 5 ml/min by applying 25 ml of water, followed by a linear gradient of 0–45 mM TFA/water formed over a total volume of 280 ml. This step was followed by column cleaning and re-equilibration wherein the column was washed with 30 ml of 100 mM aqueous TFA followed by 40 ml deionized water for re-equilibration prior to the next injection. Effluent samples that showed UV absorbance at 254 nm were collected manually.

4.2.1.4. Open-column chromatography, Method 3—preparative anion-exchange chromatography on columns of DEAE-cellulose. The DEAE-cellulose (DE-53) anion exchange chromatographic system was used for desalting, polishing, and final purification of the dinucleotides that had already been purified by the AG MP-1 column. DE-53 cellulose which was equilibrated with 100 mM NH_4HCO_3 was packed into an open glass column 2.5 cm × 30 cm (column volume = 147 ml). 200 ml of deionized water was applied to the column until the pH of the effluent, which was previously at pH 8, was neutral. The dry sample of dinucleotide and any residual salts was diluted to 1 mg/15 ml and loaded onto the column. The separation was developed by the application of a linear gradient formed between 250 ml of water and 250 ml of 800 mM NH_4HCO_3 at a flow rate of 2 ml/min using a slight positive pressure generated by a peristaltic pump. Fractions were collected and monitored for absorbance at 254 nm. Fractions that showed absorbance at this wavelength were combined, frozen and lyophilized.

*4.2.2. Synthesis and characterization of new compounds **4**, **5** and **8***

*4.2.2.1. 5-(3-(3-Azido-5-(azidomethyl) benzamido)propyl) nicotinic acid **(4)***. A 10 ml vial was wrapped in an aluminum foil and equipped with a stirring bar. Compound **8** (500 mg, 1.22 mmol) was dissolved in 5 ml of 1:1 CH_3OH-tetrahydrofuran (THF) solution and stirred at room temperature. 4 N KOH (1 ml) was added dropwise to the reaction mixture and stirred for 4 h. At this time TLC (CH_3OH-CH_2Cl_2-acetic acid 9:90:1) indicated the consumption of the starting material. HCl (1 M, 4 ml) was added to the reaction mixture and stirring continued for another 10 min. The solvents in the reaction mixture were distilled *in vacuo* and the resulting residue was purified by column chromatography on C-18 column using Combiflash R_f system (0–60% CH_3OH-H_2O) and the product collected and dried *in vacuo* to afford an off-white oil (279.3 mg, 60%). TLC C-18 alumina backed TLC plates (RP18, Analtech (Newark, DE) cat# 350016) R_f 0.38 in 50% CH_3OH-H_2O, ^{1}H NMR (600 MHz, D_2O with water suppression) δ 8.52 (s, 1 H), 8.35 (s, 1 H), 8.02 (s, 1 H), 7.17(s, 1 H), 7.14(s, 1 H), 7.06 (s, 1 H), 4.36 (s, 2 H), 3.38 (t, 2H, J = 6.18 Hz), 2.74 (t, 2H, J = 7.08 Hz), 1.99 (p, 2H, J = 6.60 Hz); ^{13}C NMR (150.9 MHz, CD_3OD) δ 167.3, 167.2, 152.2, 147.5, 141.2, 138.6, 137.5, 137.0, 136.5, 127.2, 123.0, 121.0, 117.1, 53.3, 39.2, 30.1, 29.7.

*4.2.2.2. 5-[3-(3-Azido-5-(azidomethyl)benzamido)propyl]-NAADP **(5)***. A 10 ml vial was wrapped in an aluminum foil and equipped with a stirring bar. 5-[3-(3-Azido-5-(azidomethyl)benzamido)propyl]-nicotinic acid **(4)** (68.4 mg, 0.18 mmol) was dissolved in distilled water (5 ml) and transferred to the 10 ml vial. The reaction mixture was continuously stirred for 30 min in an incubator (37 °C). After this time the pH was adjusted to 7 with 0.1–0.5 M NaOH and stirred for another 10 min. This procedure was repeated until the pH was stabilized to 7. After the pH was stabilized, NADP (10 mg, 0.01 mmol) was added to the vial and stirred at 37 °C for 10 min. Next, mutant E98G, *Aplysia californica* ADP-ribosyl cyclase (180 µl, 18 µg) was added to the reaction solution and stirred at 37 °C for 3.5 h. Analysis by HPLC (method 1) indicated the consumption of NADP after 3.5 h. The sample was then purified by preparative HPLC according to method 2. 5-[3-(3-Azido-5-(azidomethyl)-benzamido)propyl]-NAADP (**5**) eluted between 37 and 45 min (40–45 % B). The fractions collected from the HPLC were combined and pH of solution was adjusted to 7 using 0.1–1 M NaOH. The neutral solution was frozen at −80 °C protected from light by a covering of aluminum foil and lyophilized to give a white amorphous residue. Next, the dry residue was dissolved in 150 ml water and then loaded onto the DEAE-cellulose anion exchange column for further purification according to method 3. The fractions that displayed a UV absorbance at 254 nm were collected, frozen at −80 °C and lyophilized to afford a white powder: (4.2 mg, 34.9%). ^{1}H NMR (600 MHz, D_2O with water suppression) δ 8.79 (s, 1 H), 8.72 (s, 1 H), 8.54 (s, 1 H), 8.20 (s, 1 H), 7.90 (s, 1 H), 7.13 (s, 1 H), 6.99 (m, 2 H), 5.86 (d, 1H, J = 5.16 Hz), 5.82 (d, 1H, J = 5.16 Hz), 4.37 (t, 1H, J = 5.04 Hz), 4.35 (m, 1 H), 4.24-3.99 (m, 8 H), 3.28 (tt, 2H, J = 6.60 Hz), 2.80 (t, 2H, J = 7.44 Hz), 1.90 (p, 2H, J = 6.84 Hz); ^{31}P NMR (161.9 MHz, D_2O) δ 0.52, -10.74 (dd). HRMS calcd for $C_{32}H_{39}N_{13}O_{19}P_3^+$: 1002.1698, Found *m/z*: 1002.1694 (M^+). HPLC Method 1: t = 25–32 min, 32 mM TFA; UV absorption spectrum: λ_{max} 253 nm, $\varepsilon_{253} = 2.78 \times 10^{+4}$ L mol^{-1} cm^{-1}; $\varepsilon_{260} = 2.57 \times 10^{+4}$ L mol^{-1} cm^{-1}; $\varepsilon_{280} = 7.16 \times 10^{+3}$ L mol^{-1} cm^{-1}.

*4.2.2.3. Determination of the extinction coefficients of AIOC-NAADP **(5)***. Solutions of **5** were prepared, the absorption spectrum measured, and the concentrations of the dinucleotide determined by measurement of the quantity of organic phosphate in a 100 µl aliquot according to the method of Ames, 1966 [62].

*4.2.2.4. Ethyl-5-[3-(3-azido-5-(azidomethyl)benzamido)propyl]nicotinate **(8)***. A 10 ml vial was wrapped in an aluminum foil and equipped with a stirring bar. Compound **6**, 3-azido-5-azidomethylbenzoic acid (190.6 mg, 0.87 mmol) was dissolved in THF (5 ml) and N-hydroxysuccinimide (109.6 mg, 0.95 mmol) added and stirred for 10 min at room temperature. Compound **7** (ethyl 5-(3-aminopropyl) nicotinate) [28] (199.8 mg, 0.96 mmol), diisopropylcarbodiimide (163.8 mg, 1.29 mmol) and diisopropylethylamine (589.4 mg, 4.56 mmol) were added consecutively and the reaction mixture was stirred continuously at room temperature for 16 h. At this time, TLC showed the total consumption of the starting material and a distinct new spot at an R_f of 0.33 (silica gel, ethyl acetate) The reaction mixture was concentrated *in vacuo*, and the concentrated residue was purified by column chromatography on silica gel (0–10% CH_3OH-DCM) affording a yellow oil. For analytical purposes, compound **8** was crystallized from ethyl acetate to afford needle like colorless crystals. (226.4 mg, 63.5%). TLC R_f 0.33 in ethyl acetate (100%), ^{1}H NMR (600 MHz, $CDCl_3$) δ 9.08 (d, 1H, J = 1.98 Hz), 8.64 (d, 1H, J =

2.16 Hz), 8.15 (t, 1H, J = 2.10 Hz), 7.44 (s, 1 H), 7.41 (t, 1H, J = 1.86 Hz), 7.11 (q, 1H, J = 1.56 Hz), 6.36 (t, 1H, -NH, J = 5.22 Hz), 4.43 (q, 2H, J = 7.14 Hz), 4.42 (s, 2 H), 3.55 (q, 2H, J = 6.30 Hz), 2.80 (dd, 2H, J = 7.62 Hz), 2.02 (quintuplet, 2H, J = 7.74 Hz), 1.43 (t, 3H, J = 7.14 Hz); ^{13}C NMR (150.9 MHz, $CDCl_3$) δ 166.3, 165.4, 153.4, 148.8, 141.5, 138.2, 136.9, 136.7, 136.5, 126.1, 122.5, 121.2, 117.5, 72.5, 53.5, 39.5, 20.5, 20.0, 17.0. HRMS calcd for $C_{19}H_{20}N_8O_3$: 409.1737 ((M + H)). Found 409.1739 ((M + H)). Anal. calcd for $C_{19}H_{20}N_8O_3 \cdot$ ¼ EtOAc: C, 55.81; H, 5.15; N, 26.03. Found: C, 55.49; H, 4.98; N, 26.18.

4.2.3. Radiochemical synthesis

[^{32}P]-NAADP (**1**), [^{32}P]-5-N_3-NAADP (**2**) and [^{32}P]-AIOC-NAADP (**5**) — The [^{32}P]-labeled probes were synthesized using a two-step strategy used previously [34]. In the first step, [^{32}P]-NAD is converted to [^{32}P]-NADP using human recombinant NAD kinase (Enzo Life Sciences, Farmingdale, NY; ALX-201-236). The resulting [^{32}P]-NADP is converted to the appropriate probe through a base-exchange reaction catalyzed by wild type [24] or a mutant E98 G *Aplysia* ADP-ribosyl cyclase [42]. The conditions for each base-exchange reaction for the production of each probe are detailed below. The [^{32}P]-NADP was dried in a Savant SpeedVac concentrator prior to the base-exchange reactions.

[^{32}P]-NAADP was produced by adding 200 µl of 50 mM nicotinic acid in 100 mM sodium acetate, pH 4 to a vial of dried [^{32}P]-NADP. The reaction was started by adding 0.5 µl of 0.1 mg/ml wild type *Aplysia* ADP-ribosyl cyclase and allowed to incubate for 2 h at room temperature in the dark.

[^{32}P]-5-N_3-NAADP was produced by adding 100 µl of 50 mM 5-N_3-nicotinic acid, pH 7 to a vial of dried [^{32}P]-NADP. The reaction was started by adding 0.5 µl of 0.1 mg/ml E98 G *Aplysia* ADP-ribosyl cyclase and allowed to incubate for 5 h at room temperature in the dark. The E98 G ADP-ribosyl cyclase mutant is able to catalyze the base-exchange reaction at neutral pH, which is useful in situations where the nicotinic acid analog being used in not soluble at pH 4 [42].

[^{32}P]-AIOC-NAADP was produced by adding 50 µl of 50 mM AIOC-nicotinic acid, pH 7.5 to a dried aliquot of [^{32}P]-NADP. The reaction was started by adding 1 µl of 0.1 mg/ml E98 G *Aplysia* ADP-ribosyl cyclase and allowed to incubate at room temperature in the dark for 5 h. All reactions were purified by chromatography on a AG MP-1 column as previously described [34].

4.2.4. Photoaffinity labeling studies

The conditions for the preparation of sea urchin egg homogenates and their photoaffinity labeling has been previously described [34–36]. Jurkat and SKBR3 cell extracts were prepared as previously described [35,36]. Briefly, whole cell lysates (WCL) were prepared by resuspension of trypsinized or pelleted cells in HEPES buffer (20 mM HEPES, protease inhibitors (Roche), pH 7.3) prior to sonication on ice. The sonicated sample was then centrifuged (1000 × g for 10 min, 4 °C) and the pellet discarded. The cytosolic fraction was prepared from the WCL by dual centrifugation steps. Supernatant from a second spin (10,000*g* for 20 min, 4 °C) was collected and re-spun (100,000*g* for 1 h, 4 °C) to yield the cytosolic cell extract that was used for photoaffinity labeling in this study.

The standard labeling condition utilized 0.3–3 nM ^{32}P- probe (5-N_3-NAADP or AIOC-NAADP). Samples were incubated with [^{32}P] -photoprobe for 5–90 min on ice prior to photoactivation effected by exposure of samples to UV light for 2 min. PAL samples were then incubated (< 15 min) with SDS sample buffer supplemented with 2-mercaptoethanol (10%) to reduce free label. The photolabeled samples were analyzed by SDS-PAGE on 12% TGX gels from Bio-Rad. The resulting gels were stained with Simply Blue Safestain and air-dried. The photolabeling was analyzed by exposing the dried gels to MP storage phosphor screens (Packard Instruments). The screens were developed using a Typhoon storage phosphor system. Densitometric analysis was accomplished using Image *J* software.

4.2.5. Click chemistry conditions

Jurkat cell extracts photoaffinity labeled with AIOC-NAADP was subjected to click chemistry in order to determine if proteins photocrosslinked were able to be biotinylated (results shown in Fig. 10). Jurkat cytosol was first photoaffinity labeled with either unlabeled AIOC-NAADP or [^{32}P]-AIOC-NAADP in separate reactions. The photoaffinity labeling reactions were done in a total volume of 480 µl containing 1.5 mg/ml Jurkat cytosol and either 100 nM unlabeled AIOC-NAADP or 1 nM [^{32}P]-AIOC-NAADP (**5**). Following the UV irradiation under the standard photolabeling protocol, the two samples were mixed and desalted using Roche Quick Spin Columns (Sephadex G-25) to remove free probe. The desalted sample (2.3 ml) was divided into five equal (460 µl) aliquots and subjected to either copper(I) catalyzed click chemistry or strain promoted click chemistry. Diazo-biotin-alkyne, acetylene-PEG-biotin, Diazo-biotin-DBCO and DBCO-PEG4-biotin and THPTA were obtained from Click Chemistry Tools, Phoenix, AZ. The copper(I) catalyzed click chemistry conditions were performed under conditions optimized by Finn, Banyon, McKart and colleagues [63,64]. Each reaction contained 72 µM diazo-biotin-alkyne or acetylene-PEG-biotin, 5 mM aminoguanidine, 0.1 mM $CuSO_4$, 0.5 mM THPTA and 5 mM ascorbic acid in a total volume of 530 µl (460 µl of desalted photolyzed sample). The $CuSO_4$ and THTPA were mixed in a 1:5 ratio just prior to addition. The reactions were allowed to proceed 2 h at room temperature. The strain promoted click chemistry reactions were performed as follows. Diazo-biotin-DBCO or DBCO-PEG4-biotin were added to 460 µl of the desalted photolyzed Jurkat sample to a final concentration of 36 µM and incubated at room temperature for 16 h. The fifth aliquot of desalted photolyzed Jurkat cytosol sample served as a control. The click reagents were removed after the reaction by desalting as described above. The control and desalted samples from the four click reactions were then allowed to incubate with 200 µl of streptavidin-agarose (SAA) beads for 16 h at 4 °C on a rotator. The samples were then centrifuged at 4000 rpm for 2 min and the supernatant was removed and the SAA pellets were washed 5 times with 5 ml of phosphate-buffered saline (PBS), pH 7.4. The final washed SAA pellets were suspended in 2 × SDS sample buffer and boiled for 20 min to release proteins bound to the SAA beads. The SAA beads were transferred to a Costar SpinS centrifugal filter unit and centrifuged to remove the SAA beads. The proteins released were analyzed by SDS-PAGE on 12% TGX gels from Bio-Rad.

Funding

J.T.S. and T.F.W. acknowledge financial support from NIH Institute of General Medical Sciences Grants R15-GM100444 and R15-GM131329. Work at the University of Toledo was partially supported by The University of Toledo Foundation Cancer Research Support Account. J.S.M. and G.S.G. acknowledge financial support from NIHR01-GM088790.

Author contributions

All authors contributed to this work, and all have approved this manuscript. The results presented in this study are taken, in part, from the dissertation submitted by Timnit Y. Asfaha to The University of Toledo College of Graduate Studies for the Ph.D. degree in Medicinal Chemistry, December 2016.

Declaration of Competing Interest

The authors declare no competing financial interest.

Acknowledgements

We wish to thank Ms. Peiling Su for performing the phosphate analyses on AIOC-NAADP (**5**).

Appendix A. Supplementary data

Supplementary material related to this article can be found, in the online version, at doi:https://doi.org/10.1016/j.ceca.2019.102060.

References

[1] J.K. Jaiswal, Calcium - how and why? J. Biosci. 26 (2001) 357–363.
[2] M.P. Mattson, S.L. Chan, Calcium orchestrates apoptosis, Nat. Cell Biol. 5 (2003) 1041–1043.
[3] A. Raffaello, C. Mammucari, G. Gherardi, R. Rizzuto, Calcium at the center of cell signaling: interplay between endoplasmic reticulum, mitochondria, and lysosomes, Trends Biochem. Sci. 41 (2016) 1035–1049.
[4] M.J. Berridge, Calcium signaling remodelling and disease, Biochem. Soc.Trans. 40 (2012) 297–309.
[5] M.J. Berridge, P. Lipp, M.D. Bootman, The versatility and universality of calcium signalling, Nat. Rev. Mol. Cell Biol. 1 (2000) 11–21.
[6] H.C. Lee, Nicotinic acid adenine dinucleotide phosphate (NAADP)-mediated calcium signaling, J. Biol. Chem. 280 (2005) 33693–33696.
[7] H.C. Lee, R. Aarhus, A derivative of NADP mobilizes calcium stores insensitive to inositol trisphosphate and cyclic ADP-ribose, J. Biol. Chem. 270 (1995) 2152–2157.
[8] A. Galione, A primer of NAADP-mediated Ca^{2+} signalling: from sea urchin eggs to mammalian cells, Cell Calcium 58 (2015) 27–47.
[9] A.H. Guse, Second messenger signaling: multiple receptors for NAADP, Curr. Biol. 19 (2009) R521–523.
[10] H.C. Lee, Cyclic ADP-ribose and nicotinic acid adenine dinucleotide phosphate (NAADP) as messingers for calcium mobilization, J. Biol. Chem. 287 (2012) 31633–31640.
[11] M. Albrieux, H.C. Lee, M. Villaz, Calcium signaling by cyclic ADP-ribose, NAADP, and inositol trisphosphate are involved in distinct functions in ascidian oocytes, J. Biol. Chem. 273 (1998) 14566–14574.
[12] J.M. Cancela, G.C. Churchill, A. Galione, Coordination of agonist-induced Ca^{2+}-signalling patterns by NAADP in pancreatic acinar cells, Nature 398 (1999) 74–76.
[13] G.C. Churchill, J.S. O'Neill, R. Masgrau, S. Patel, J.M. Thomas, A.A. Genazzani, A. Galione, Sperm deliver a new second messenger: NAADP, Curr. Biol. 13 (2003) 125–128.
[14] B. Schomer, D. Epel, Redox changes during fertilization and maturation of marine invertebrate eggs, Dev. Biol. 203 (1998) 1–11.
[15] P.K. Aley, H.J. Noh, X. Gao, A.A. Tica, E. Brailoiu, G.C. Churchill, A functional role for nicotinic acid adenine dinucleotide phosphate in oxytocin-mediated contraction of uterine smooth muscle from rat, J. Pharmacol. Exp. Ther. 333 (2010) 726–735.
[16] E. Brailoiu, J.L. Hoard, C.M. Filipeanu, G.C. Brailoiu, S.L. Dun, S. Patel, N.J. Dun, Nicotinic acid adenine dinucleotide phosphate potentiates neurite outgrowth, J. Biol. Chem. 280 (2005) 5646–5650.
[17] A. Arredouani, A.M. Evans, J. Ma, J. Parrington, M.X. Zhu, A. Galione, An emerging role for NAADP-mediated Ca^{2+} signaling in the pancreatic beta-cell, Islets 2 (2010) 323–330.
[18] A. Arredouani, M. Ruas, S.C. Collins, R. Parkesh, F. Clough, T. Pillinger, G. Coltart, K. Rietdorf, A. Royle, P. Johnson, M. Braun, Q. Zhang, W. Sones, K. Shimomura, A.J. Morgan, A.M. Lewis, K.T. Chuang, R. Tunn, J. Gadea, L. Teboul, P.M. Heister, P.W. Tynan, E.A. Bellomo, G.A. Rutter, P. Rorsman, G.C. Churchill, J. Parrington, A. Galione, Nicotinic acid adenine dinucleotide phosphate (NAADP) and endolysosomal two-pore channels modulate membrane excitability and stimulus-secretion coupling in mouse pancreatic beta cells, J. Biol. Chem. 290 (2015) 21376–23192.
[19] C. Cordiglieri, F. Odoardi, B. Zhang, M. Nebel, N. Kawakami, W.E. Klinkert, D. Lodygin, F. Luhder, E. Breunig, D. Schild, V.K. Ulaganathan, K. Dornmair, W. Dammermann, B.V. Potter, A.H. Guse, A. Flugel, Nicotinic acid adenine dinucleotide phosphate-mediated calcium signalling in effector T cells regulates autoimmunity of the central nervous system, Brain 133 (2010) 1930–1943.
[20] I.M. Wolf, B.P. Diercks, E. Gattkowski, F. Czarniak, J. Kempski, R. Werner, D. Schetelig, H.W. Mittrucker, V. Schumacher, M. von Osten, D. Lodygin, A. Flugel, R. Fliegert, A.H. Guse, Frontrunners of T cell activation: initial, localized Ca^{2+} signals mediated by NAADP and the type 1 ryanodine receptor, Sci. Signal. 8 (2015) ra102.
[21] R.A. Ali, C. Camick, K. Wiles, T.F. Walseth, J.T. Slama, S. Bhattacharya, D.R. Giovannucci, K.A. Wall, Nicotinic acid adenine dinucleotide phosphate plays a critical role in naive and effector murine T cells but not natural regulatory T cells, J. Biol. Chem. 291 (2016) 4503–4522.
[22] C. Bernofsky, Nicotinic acid adenine dinucleotide phosphate, Methods Enzymol. 66 (1980) 105–112.
[23] R. Aarhus, R.M. Graeff, D.M. Dickey, T.M. Walseth, H.C. Lee, ADP-ribosyl cyclase and CD38 catalyze the synthesis of a calcium-mobilizing metabolite form $NADP^{(+)}$, J. Biol. Chem. 270 (1995) 30327–30333.
[24] C. Munshi, H.C. Lee, High-level expression of recombinant *Aplysia* ADP-ribosyl cyclase in *Pichia pastoris* by fermentation, Protein Expression Purif. 11 (1997) 104–110.
[25] R.A. Billington, G.C. Tron, S. Reichenbach, G. Sorba, A.A. Genazzani, Role of the nicotinic acid group in NAADP receptor selectivity, Cell Calcium 37 (2005) 81–86.
[26] P. Jain, J.T. Slama, L.A. Perez-Haddock, T.F. Walseth, Nicotinic acid adenine dinucleotide phosphate analogues containing substituted nicotinic acid: effect of modification on Ca^{2+} release, J. Med. Chem. 53 (2010) 7599–7612.
[27] H.C. Lee, R. Aarhus, Structural determinants of nicotinic acid adenine dinucleotide phosphate important for its caclium-mobilizing activity, J. Biol. Chem. 272 (1997) 20378–20383.
[28] C.J. Trabbic, F. Zhang, T.F. Walseth, J.T. Slama, Nicotinic acid adenine dinucleotide phosphate analogues substituted on the nicotinic acid and adenine ribosides. Effects on receptor mediated $Ca^{(2+)}$ release, J. Med. Chem. 58 (2015) 3593–3610.
[29] H.C. Lee, R. Aarhus, Functional visualization of the separate but interacting calcium stores sensitive to NAADP and cyclic ADP-ribose, J. Cell. Sci. 113 (Pt 24) (2000) 4413–4420.
[30] G.C. Churchill, Y. Okada, J.M. Thomas, A.A. Genazzani, S. Patel, A. Galione, NAADP mobilizes $Ca^{(2+)}$ from reserve granules, lysosome-related organelles, in sea urchin eggs, Cell 111 (2002) 703–708.
[31] P.J. Calcraft, M. Ruas, Z. Pan, X. Cheng, A. Arredouani, X. Hao, J. Tang, K. Rietdorf, L. Teboul, K.T. Chuang, P. Lin, R. Xiao, C. Wang, Y. Zhu, Y. Lin, C.N. Wyatt, J. Parrington, J. Ma, A.M. Evans, A. Galione, M.X. Zhu, NAADP mobilizes calcium from acidic organelles through two-pore channels, Nature 459 (2009) 596–600.
[32] M. Hohenegger, J. Suko, R. Gscheidlinger, H. Drobny, A. Zidar, Nicotinic acid-adenine dinucleotide phosphate activates the skeletal muscle ryanodine receptor, Biochem. J. 367 (2002) 423–431.
[33] F. Zhang, P.L. Li, Reconstitution and characterization of a nicotinic acid adenine dinucleotide phosphate (NAADP)-sensitive Ca^{2+} release channel from liver lysosomes of rats, J. Biol. Chem. 282 (2007) 25259–25269.
[34] T.F. Walseth, Y. Lin-Moshier, P. Jain, M. Ruas, J. Parrington, A. Galione, J.S. Marchant, J.T. Slama, Photoaffinity labeling of high affinity nicotinic acid adenine dinucleotide phosphate (NAADP)-binding proteins in sea urchin egg, J. Biol. Chem. 287 (2012) 2308–2315.
[35] Y. Lin-Moshier, T.F. Walseth, D. Churamani, S.M. Davidson, J.T. Slama, R. Hooper, E. Brailoiu, S. Patel, J.S. Marchant, Photoaffinity labeling of nicotinic acid adenine dinucleotide phosphate (NAADP) targets in mammalian cells, J. Biol. Chem. 287 (2012) 2296–2307.
[36] T.F. Walseth, Y. Lin-Moshier, K. Weber, J.S. Marchant, J.T. Slama, A.H. Guse, Nicotinic acid adenine dinucleotide 2-phosphate (NAADP) binding proteins in T-lymphocytes, Messenger 1 (2012) 86–94.
[37] T. Hosoya, T. Hiramatsyu, T. Ikemoto, H. Aoyama, T. Ohmae, M. Endo, M. Suzuki, Design of dantrolene-derived probes for radioisotope-free photoaffinity labeling of proteins involved in the physiological Ca^{2+} release form sarcoplasmic reticulum of skeletal muscle, Bioorg. Med. Chem. Lett. 15 (2005) 1289–1294.
[38] T. Hosoya, T. Hiramatsyu, T. Ikemoto, M. Nakanishi, H. Aoyama, A. Hosoya, T. Iwata, K. Maruyama, M. Endo, M. Suzuki, Novel bifunctional probe for radioisotope-free photoaffinity labeling:compact structure comprised of photospecific ligand ligation and detectable tag anchoring units, Org. Biomol. Chem. 2 (2004) 637–641.
[39] R. Neelarapu, D.L. Holzle, S. Velaparthi, H. Bai, M. Brunsteiner, S.Y. Blond, P.A. Petukhov, Design, synthesis, docking, and biological evaluation of novel diazide-containing isoxazole- and pyrazole-based histone deacetylase probes, J. Med. Chem. 54 (2011) 4350–4364.
[40] S. Yoshida, Y. Misawa, T. Hosoya, Formal C-H-Azidation-based shortcut to diazido building blocks for the versatile preparation of photoaffinity labeling probes, Eur. J. Org. Chem. (2014) 3991–3995.
[41] R. Graeff, Q. Liu, I.A. Kriksunov, Q. Hao, H.C. Lee, Acidic residues at the active sites of CD38 and ADP-ribosyl cyclase determine nicotinic acid adenine dinucleotide phosphate (NAADP) synthesis and hydrolysis activities, J. Biol. Chem. 281 (2006) 28951–28957.
[42] C. Munshi, D.J. Thiel, I.I. Mathews, R. Aarhus, T.F. Walseth, H.C. Lee, Characterization of the active site of ADP-ribosyl cyclase, J. Biol. Chem. 274 (1999) 30770–30777.
[43] E. Brailoiu, D. Churamani, X. Cai, M.G. Schrlau, G.C. Brailoiu, X. Gao, R. Hooper, M.J. Boulware, N.J. Dun, J.S. Marchant, S. Patel, Essential requirement for two-pore channel 1 in NAADP-mediated calcium signaling, J. Cell Biol. 186 (2009) 201–209.
[44] G.C. Brailoiu, T.I. Oprea, P. Zhao, M.E. Abood, E. Brailoiu, Intracellular cannabinoid type 1 (CB1) receptors are activated by anandamide, J. Biol. Chem. 286 (2011) 29166–29174.
[45] A.J. Morgan, A. Galione, Investigating cADPR and NAADP in intact and broken cell preparations, Methods 46 (2008) 194–203.
[46] A.J. Morgan, A. Galione, Preparation and use of sea urchin egg homogenates, Methods Mol. Biol. 1128 (2014) 161–173.
[47] R. Aarhus, D.M. Dickey, R.M. Graeff, K.R. Gee, T.F. Walseth, H.C. Lee, Activation and inactivation of Ca^{2+} release by $NAADP^{+}$, J. Biol. Chem. 271 (1996) 8513–8516.
[48] A.A. Genazzani, R.M. Empson, A. Galione, Unique inactivation properties of NAADP-sensitive Ca^{2+} release, J. Biol. Chem. 271 (1996) 11599–11602.
[49] I. Berg, B.V. Potter, G.W. Mayr, A.H. Guse, Nicotinic acid adenine dinucleotide phosphate ($NAADP^{+}$) is an essential regulator of T-lymphocyte Ca^{2+}-signaling, J. Cell Biol. 150 (2000) 581–588.
[50] W. Dammermann, A.H. Guse, Functional ryanodine receptor expression is required for NAADP-mediated local Ca^{2+} signaling in T-lymphocytes, J. Biol. Chem. 280 (2005) 21394–21399.
[51] W. Dammermann, B. Zhang, M. Nebel, C. Cordiglieri, F. Odoardi, T. Kirchberger, N. Kawakami, J. Dowden, F. Schmid, K. Dornmair, M. Hohenegger, A. Flugel, A.H. Guse, B.V. Potter, NAADP-mediated Ca^{2+} signaling via type 1 ryanodine receptor in T cells revealed by a synthetic NAADP antagonist, Proc. Natl. Acad. Sci. U. S. A. 106 (2009).
[52] A. Gasser, S. Bruhn, A.H. Guse, Second messenger function of nicotinic acid adenine dinucleotide phosphate revealed by an improved enzymatic cycling assay, J. Biol. Chem. 281 (2006) 16906–16913.
[53] A.E. Speers, B.F. Cravatt, Profiling enzyme activities in vivo using click chemistry methods, Chem. Biol. 11 (2004) 535–546.
[54] R. van Geel, G.J.M. Pruijn, F.L. van Delft, W.C. Boelens, Preventing thiol-yne

addition improves the specificity of strain-promotes azide-alkyne cycloaddition, Bioconjugate Chem. 23 (2012) 392–398.
[55] R.A. Ali, T. Zhelay, C.J. Trabbic, T.F. Walseth, J.T. Slama, D.R. Giovannucci, K.A. Wall, Activity of nicotinic acid substituted nicotinic acid adenine dinucleotide phosphate (NAADP) analogs in a human cell line: difference in specificity between human and sea urchin NAADP receptors, Cell Calcium 55 (2014) 93–103.
[56] G.S. Gunaratne, P. Su, J.S. Marchant, J.T. Slama, T.F. Walseth, 5-Azido-8-ethynyl-NAADP: a bifunctional, clickable photoaffinity probe for the identification of NAADP receptors, Biochim. et Biophys. Acta. Mol. Cell Res. 1866 (2019) 1180–1188.
[57] G.G. Gordon, C.R. Berttozzi, *In vivo* applications of bioorthogonal chemistries, *In vivo* applications of bioorthogonal chemistries, in: P.E. Algar, P.E. Dawson, I.L. Medintz (Eds.), Chemoselective and Bioorthogonal Ligation Reactions: Concepts and Applications, Wiley-VCH Verlag BmbH and Co. KGaA., Weinheim, Germany, 2017, pp. 417–457.
[58] M. Meldal, C.W. Tornoe, Cu-catalyzed azide alkyne cycloaddition, Chem. Rev. 108 (2008) 2952–3015.
[59] Y. Lin-Moshier, M.V. Keebler, R. Hooper, M.J. Boulware, X. Liu, D. Churamani, M.E. Abood, T.F. Walseth, E. Brailoiu, S. Patel, J.S. Marchant, The two-pore channel (TPC) interactome unmasks isoform-specific roles for TPCs in endolysosomal morphology and cell pigmentation, Proc. Natl. Acad. Sci. U. S. A. 111 (2014) 13087–13092.
[60] T.W. Chen, T.J. Wardill, Y. Sun, S.R. Pulver, S.L. Renninger, A. Baohan, E.R. Schreiter, R.A. Kerr, M.B. Orger, V. Jayaraman, L.L. Looger, K. Svoboda, D.S. Kim, Ultrasensitive fluorescent proteins for imaging neuronal activity, Nature 499 (2013) 295–300.
[61] A.J. Lam, F. St-Pierre, Y. Gong, J.D. Marshall, P.J. Cranfill, M.A. Baird, M.R. McKeown, J. Wiedenmann, M.W. Davidson, M.J. Schnitzer, R.Y. Tsien, M.Z. Lin, Improving FRET dynamic range with bright green and red fluorescent proteins, Nat. Methods 9 (2012) 1005–1012.
[62] B.M. Ames, Assay of inorganic phosphate, total phosphate, and phosphatases, Methods Enzymol. 8 (1966) 115–118.
[63] V. Hong, S.I. Presolski, C. Ma, M.G. Finn, Analysis and optimization of copper-catalyzed azide-alkyne cycloaddition for bioconjugation, Angew. Chem. Int. Ed. Engl. 48 (2009) 9879–9883.
[64] S.I. Presolski, V.P. Hong, M.G. Finn, Copper-catalyzed azide-alkyne click chemistry for bioconjugation, Curr. Protoc. Chem. Biol. 3 (2011) 153–162.